

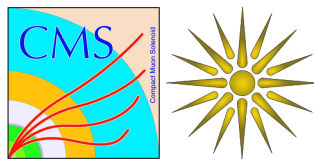
Performance and calibration of CASTOR calorimeter at CMS

Mykola Savitskyi, Taras Shevchenko National University of Kyiv, Ukraine

September 8, 2011

Abstract

Calibration of the relative response of every individual channel of the CASTOR calorimeter of the CMS detector was performed by analyzing halo muons events collected during the LHC operation at March-April 2011. Intercalibration constants obtained from that period of data taking were compared to previous results from 2010.



Contents

1	Introduction	3
2	Overview	3
2.1	CASTOR physics	3
2.2	CASTOR design	4
2.2.1	Fine-mesh PMTs	5
2.2.2	Front-end electronics	6
2.2.3	Influence of the residual magnetic field	6
3	Intercalibration	7
3.1	Halo muons	7
3.1.1	Trigger	8
3.2	Event selection	8
3.2.1	Data sample and statistics	9
3.3	Spectra comparison	10
3.4	Intercalibration constants	10
3.5	Discussion of the results	11
3.5.1	Validation of selection for 2011 analysis	11
3.5.2	Influence of the selection criteria	11
3.5.3	Update of the selection criteria for 2011 analysis	11
3.5.4	Comparison of intercalibration constants	12
4	Summary and conclusions	12

1 Introduction

The CASTOR very forward Cherenkov sampling calorimeter is a unique detector that covers a phase-space region that has never been explored before. CASTOR has a very rich physics program at proton-proton and heavy ion forward physics.

Here I focus on the detector's general overview and intercalibration with halo muons.

2 Overview

The Compact Muon Solenoid (CMS) is a large general-purpose particle physics detector installed at the Large Hadron Collider (LHC) at CERN. General purposes of the CMS are: exploring physics at TeV scale, discovery of the Higgs boson, search for physics beyond the Standard Model (Supersymmetry, Extra Dimensions) and heavy ion physics studies.

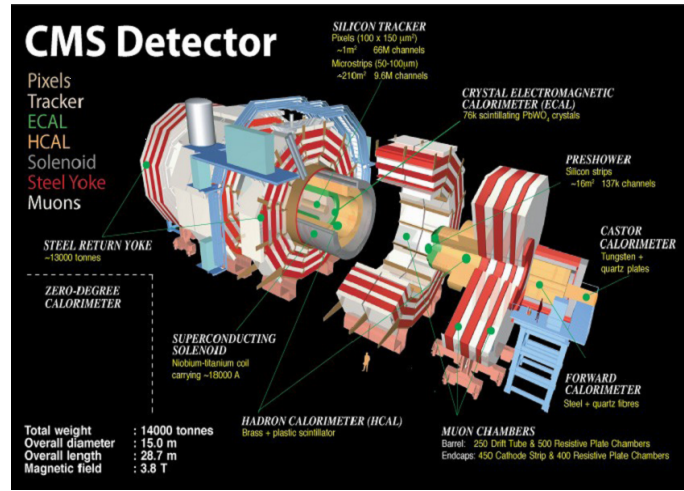


Figure 1: CMS and installed CASTOR.

CASTOR is located at the most forward region of the CMS detector, at $z \approx 14.4$ m from the interaction point, covering the pseudorapidity range $-6.6 < \eta < -5.2$, where pseudorapidity is defined as $\eta = -\ln\left[\tan\left(\frac{\theta}{2}\right)\right]$ and θ is the angle between the scattered particle momentum and the beam axis¹. CASTOR covers a phase-space region that has never been explored so far.

On Figure 1 the CMS detector layout with installed CASTOR is shown.

2.1 CASTOR physics

CASTOR (Centauro and Strange Object Research) was initially intended to be installed in a heavy-ion experiment to search for exotic objects with unusual longitudinal shower profile

¹ $-6.6 < \eta < -5.2$ corresponds to $0.2 < \theta < 0.6$

properties. Several objects of such kind were observed in cosmic-ray experiments (the so-called Centauro events) and may be also produced in heavy-ion collisions at the LHC. Since being part of the CMS detector CASTOR physics program has been extended to proton-proton collisions as well.

CASTOR will contribute to the following forward physics topics:

- p-p collisions:
 1. low- x_{Bj} ($x_{Bj} = p_{parton}/p_{hadron}$) QCD studies as a key to understand the structure of the proton
 2. constrain PDFs at $3 \cdot 10^{-5} < x_{Bj} < 2 \cdot 10^{-6}$ (14TeV)
 3. parton saturation effects
 4. DGLAP[1]/BFKL[2]/CCFM[3] dynamics
 5. multi-parton interactions and underlying event structure
 - to be performed by analyzing forward energy flow and forward jet production
 6. diffraction studies
 - to be performed by distinguishing between single/double diffractive events
- HI collisions:
 1. centrality, limiting fragmentation, elliptic flow
 2. Centauros and Strangelets (exotica)

2.2 CASTOR design

CASTOR sampling structure consisting of tungsten and quartz plates is shown in Figure 2. Tungsten, as the absorber material, provides small transverse shower size; quartz glass², as the active material, is resistant to damage from radiation. The quartz plates are tilted at 45° to capture efficiently the Cherenkov light produced by the relativistic particles passing through the detector. The Cherenkov light is collected by air-core light guides, whose inner surface is covered by a wavelength selective mirroring foil³. Light guides are connected to the photo-multiplier tubes (PMTs), which produce signals proportional to the amount of collected light.

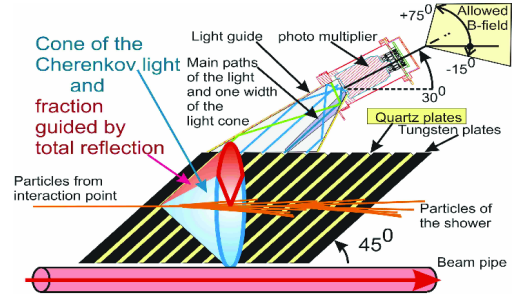


Figure 2: Sampling structure, light generation and its readout.

²Synthetic fused silica including of admixtures which enhance radiation hardness. It also has better optical properties than normal quartz: $n_{ref} = (1.46 - 1.55)$ for $\lambda = (600 - 200)nm$.

³Radiation hard reflector coated with dielectrics SiO_2, TiO_2 . The dielectrics increase the reflectance to 95% for $\lambda \sim 420nm$ while cutting light with $\lambda < 350nm$.

CASTOR is constructed as shown in Figure 3. Two stainless steel skeletons - one for each side of the beam pipe - contain 14 longitudinal sections (modules) adding up to 10 nuclear interaction lengths. Two of them are electromagnetic sections with thinner sampling structure ($X_0 \sim 20$) to distinguish electrons/photons from hadrons, while the remaining 12 are hadronic sections. In the $r - \phi$ plane the cylindrical geometry is approximated by an octagon divided into 16 individual semi-octant sectors (Figure 4). In total there are 224 read-out channels equipped with fine-mesh PMTs.

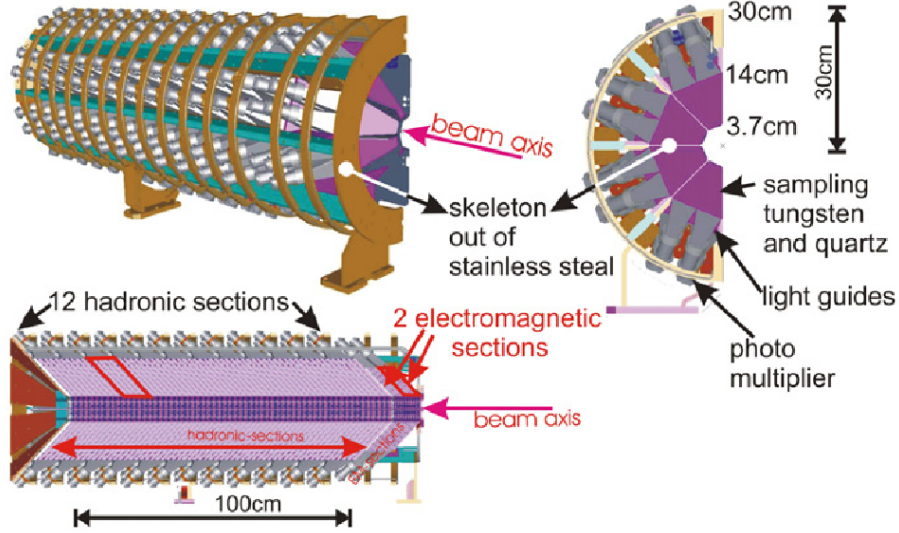


Figure 3: 3D view of CASTOR mechanical construction. Also the transversal and longitudinal profiles of the calorimeter are shown.

2.2.1 Fine-mesh PMTs

Fine-mesh PMTs have a very different geometry of the dynode⁴ chain with respect to ordinary PMTs. In their volume, mesh-type dynodes are stacked parallel to each other and perpendicular to the main PMT axis with a spacing between the dynodes of only a few millimeters (Figure 5). This setup greatly reduces the impact of external magnetic fields on the electron cascade in the PMT. The performance of fine-mesh PMTs is stable up to high values of the magnetic field flux. However, at large angles between PMT axis and the field a PMT response impairs significantly.

The signal from a fine-mesh PMT reading out a CASTOR channel can be described by the following formula:

$$Signal[e^-] = N_\gamma(E) \cdot \epsilon_{opt} \cdot QE^{PMT} \cdot G,$$

⁴A dynode is one of a series of electrodes within a photomultiplier tube. Each dynode is at a more positive electrical potential than its predecessor. Secondary emission occurs at the surface of each dynode. Such an arrangement is able to amplify the tiny current (even corresponding to one single electron emitted by the photocathode) typically by a factor of one million.

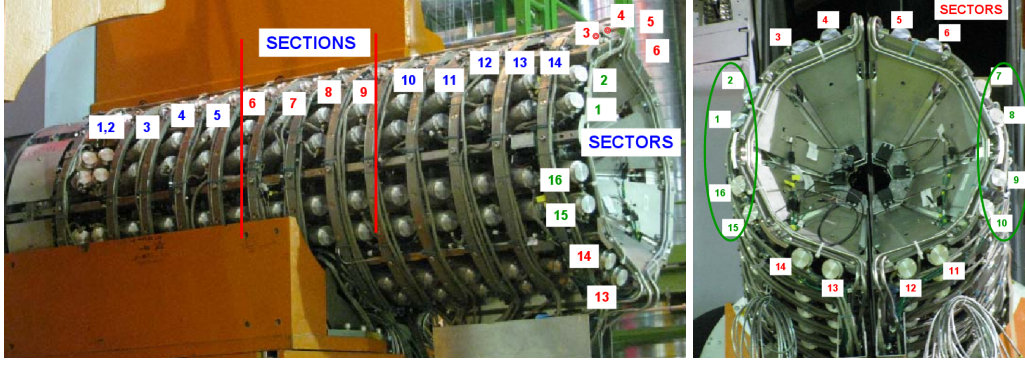


Figure 4: Longitudinal and azimuthal segmentation of CASTOR.

where N_γ is the number of Cherenkov photons produced by particle, ϵ_{opt} is the optical efficiency of the light guide, QE^{PMT} denotes the quantum efficiency of the PMT and G is the gain of the PMT ($10^4 < G < 10^5$).

2.2.2 Front-end electronics

Electronics of CMS subdetectors have to separate the signals for every LHC bunch crossing (25 ns) and manage its digitization and transfer. A signal from a CASTOR PMT is integrated and encoded with an ASIC⁵, called QIE⁶. It uses 4 capacitors to accumulate the charge in 25 ns time samples (TS). Each subsequent time sample comes from a different capacitor. Since the total signal duration is longer than 25 ns the sum of several TS is used for its reconstruction.

The following digital electronics provides streaming, calculation of trigger bits and sending of them to the L1-trigger of CMS. While waiting for the trigger decision the data are buffered and after a positive decision sent out to the central DAQ-system of CMS.

2.2.3 Influence of the residual magnetic field

Due to its very forward location, CASTOR is influenced by a strong magnetic field. CASTOR is shielded against radiation and the magnetic field. However, in the middle part of CASTOR (around module 7) a small air assembly gap is present where different parts of the shielding meet. This leads to a non-uniform magnetic field configuration inside CASTOR volume, where the magnetic field lines do not extend parallel to the beam pipe. Due to this magnetic field, the response of the PMTs is affected, as the trajectory of the accelerated electrons in the PMT is altered and therefore the gain is reduced. Modules 7,8 of the calorimeter, located closest to the assembly gap, are most affected, while module 6 is partly restored by increasing the high voltage (Figure 6). Hence a loss of almost two full modules of CASTOR occurs, despite the

⁵Application-Specific Integrated Circuit

⁶Charge Integrator and Encoder [4]

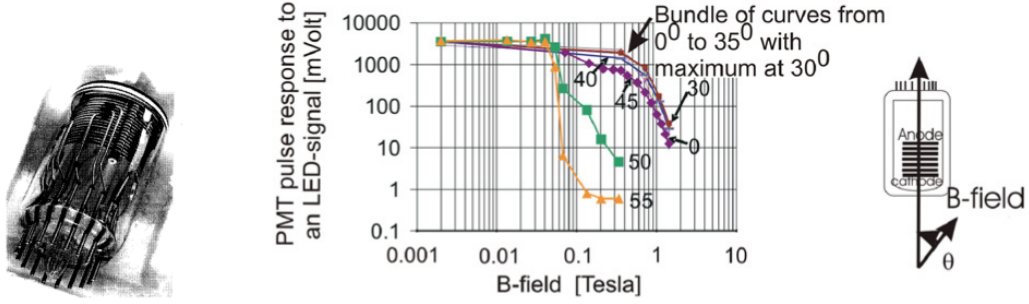


Figure 5: Left: Picture of a fine-mesh PMT, where the stack of parallel dynodes can be seen; Right: A PMT response as a function of the magnetic field measured for different angles [5].

fact that currently used fine-mesh PMTs are resistant to magnetic fields. Usage of additional μ – metal shielding is prohibited since it would induce additional mechanical force.

3 Intercalibration

As it was mentioned before, each CASTOR channel is characterized by the PMT gain and quantum efficiency and by the efficiency of light guide. An acquired signal is proportional to these constants which are individual for every channel. Thus to equalize responses of CASTOR channels the intercalibration must be performed. This is the first step towards understanding the detector performance. It is also first step towards a full calibration of CASTOR.

The intercalibration constants are used to correct for variations in the channel response within the detector, and are defined as the inverse of the ratio of each channel response to a corresponding response of a chosen reference channel. To perform intercalibration events with equal energy deposition in each CASTOR channel can be used.

3.1 Halo muons

Beam halo muons are products of proton interaction with a collimator material or beam gas⁷. Most of the halo muons are produced 50-148 m from the interaction point [6]. Thus the muons which reach the CMS area are almost parallel to the beam axis. The halo of muons is most intense close to the beam axis, where CASTOR is located. Although in physics analyses, these types of muons are generally considered as sources of background, generally they can be used for detector alignment, calibration, and detector performance validation. In a wide energy range muon energy loss is similar to the energy loss by a minimum ionizing particle. Thus a halo muon penetrates CASTOR depositing equal amount of energy in every module. It has a clear signature in the calorimeter and can be easily identified (Figure 7). To get a clean sample

⁷Rest gas in the beam pipe.

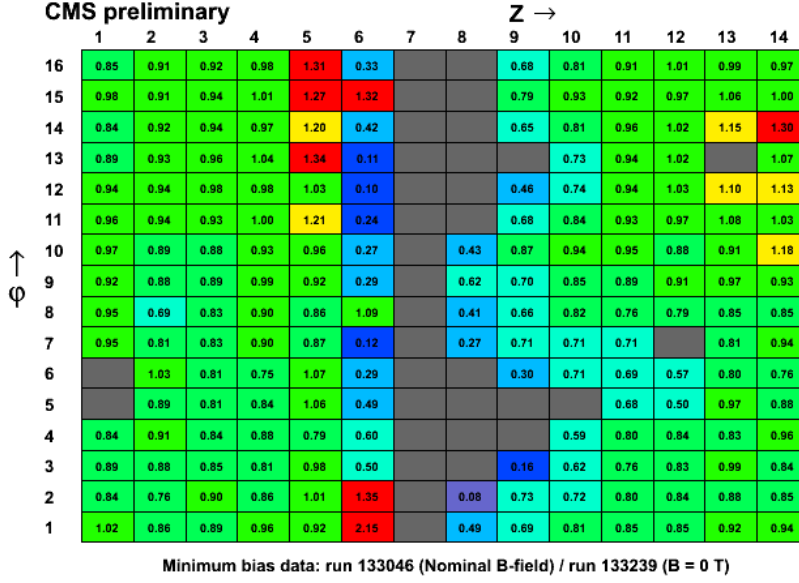


Figure 6: Left: Ratio of the average channel response measured with and without magnetic field of all channels in CASTOR. Channels shown in gray have no signals because of the magnetic field influence (mod - 7 - 10) or due to a hardware failure. Right: Assembly gap (arrow-like) between the rotating and collar shielding of CASTOR.

of halo muon events in CASTOR the data were acquired when LHC beams were circulating but not colliding.

3.1.1 Trigger

In each azimuthal sector, 4 channel triplets are considered to define a trigger condition. At least 3 triplets in a sector should have a channel with a signal above a noise threshold to fire the trigger.

3.2 Event selection

A rich sample of halo muon events is mandatory for the intercalibration of CASTOR. A special technique of event selection was used, which takes into account the structure of CASTOR, its location in non-uniform magnetic field and background events.

Data sample recorded by CMS was processed if:

- the dedicated runs were recorded during circulation of non-colliding beams:

To avoid high intensity fluxes of particles produced in collisions which do not allow a clear signature of halo muons to be distinguished.

- CASTOR trigger on an isolated penetrating particle (halo muon) was present.

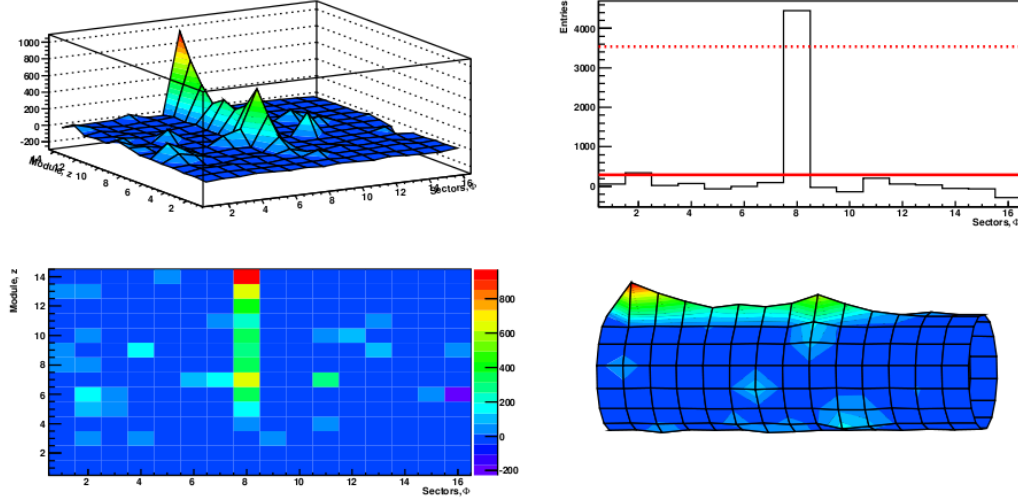


Figure 7: Example of the signature of a muon in CASTOR.

Off-line event selection:

- **isolated sector condition:**

The isolated sector condition requires that at least $CUT = N - 3$ modules in a selected sector have a signal above the noise threshold and signals from all modules in the remaining sectors are below a threshold. N , the number of working modules, varies for each sector due to the regions influenced by the magnetic field. Also this requirement helps to avoid background beam gas events and thus to improve the purity of the selected events. The importance of a proper choice of a CUT value is discussed in section 3.5.2.

- **individual module condition:**

For each preselected sector all modules are considered individually. At least $N - 3$ modules must have a signal above the noise threshold without the considered module. This condition helps to avoid bias.

3.2.1 Data sample and statistics

A sample of halo muon events was created by processing RAW DATA recorded during March-April of 2011 by CMS. The offline selection resulted in 400-2900 muons per sector, more detailed values are summarized in Table 1. This is enough to perform further intercalibration. The number of muon candidates does not scale in a simple way with the beam intensity, beam condition (Figure 8) nor with the number of bunches (bunch crossing scheme) per LHC orbit.

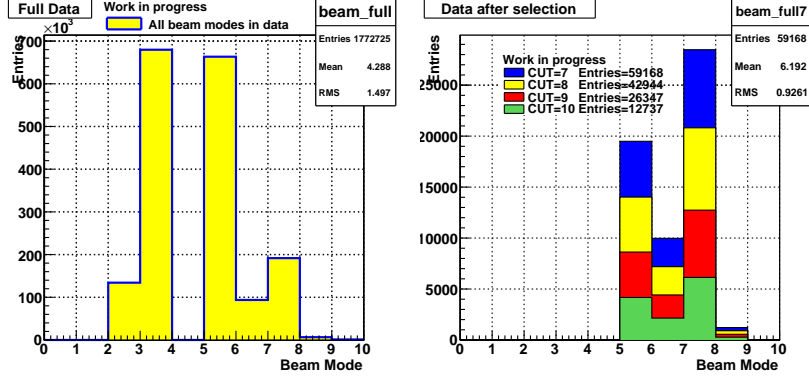


Figure 8: Muon statistics before (left) and after (right) selection during different beam modes. Most of muons are in beam modes: 5, 6, 7, 8 (beam mode bits: 1 - no mode, 2 - setup, 3 - injection of pilot bunches, 4 - intermediate injection, 5 - nominal injection, 6 - pre-ramp, 7 - ramp, 8 - flat top, 9 - squeeze, 10 - adjust).

3.3 Spectra comparison

Figure 9 shows examples of muon spectra obtained during 2010 and 2011 data taking for several CASTOR channels. The spectra are not corrected for the electronics zero shift (so-called ‘pedestal’) which is around 10 fC. The shape of spectra indicates the low photoelectron statistics of the PMT response due to the low energy deposited by a muon in a CASTOR module and due to a finite ϵ_{opt} .

3.4 Intercalibration constants

Intercalibration constants can be calculated from channel responses of the detector. They are defined individually for every channel as:

$$I_n = \left(\frac{M_n - P_n}{M_{rc} - P_{rc}} \right)^{-1},$$

where M_n - the mean value of the signal, P_n - the pedestal of the signal, M_{rc} - the mean value of the signal in the reference channel, P_{rc} - pedestal of the signal in the reference channel. The statistical error is:

$$\Delta I_n = \sqrt{\left(\frac{\Delta M_{rc}}{M_n - P_n} \right)^2 + \left(\frac{-\Delta M_n (M_{rc} - P_{rc})}{(M_n - P_n)^2} \right)^2},$$

where ΔM_{rc} is the statistical error of M_{rc} and ΔM_n is the statistical error of M_n .

Module 4 of sector 9 was chosen as a reference channel. Obviously, $I_{s9,m4}$ must be equal to 1.

Figures 10 - 11 show the M_n calculated for each channel.

Table 1: Acquired muon statistics for every channel with respect to *CUT* values.

CUT	SEC	Module													
		1	2	3	4	5	6	7	8	9	10	11	12	13	14
10	1	1586	1563	1021	1038	1000	979	2104	1165	988	1004	1012	983	1026	1022
9	2	2362	2484	1894	1884	1861	1898	2898	2627	1859	1870	1865	1870	1955	1973
8	3	1735	1765	1475	1712	1349	1445	2295	2306	1965	1405	1411	1427	1414	1515
8	4	1505	1574	1266	1294	1167	1291	2126	2134	2133	1311	1208	1181	1214	1353
7	5	673	640	536	595	513	731	1048	1101	1100	1071	516	637	560	615
8	6	1080	1052	902	972	828	984	1614	1614	1257	895	856	981	940	974
9	7	661	699	509	492	480	816	1091	790	561	525	504	482	570	518
10	8	436	451	293	272	250	292	756	374	290	244	261	257	301	249
10	9	914	1054	812	818	687	929	1507	850	765	734	705	706	725	768
9	10	1637	1709	1565	1584	1316	1788	2412	1922	1444	1412	1347	1392	1397	1439
8	11	732	936	706	549	495	712	1223	1252	590	540	1151	517	552	552
8	12	714	720	592	566	521	705	1229	1235	777	563	1188	541	532	565
8	13	722	803	615	607	563	1163	1458	1454	873	653	1389	623	602	675
8	14	1376	1517	1107	1121	1017	1211	2013	2028	1223	1064	1955	1071	1140	1145
9	15	2894	3237	2229	2191	2151	2110	3919	3917	2231	2125	2156	2176	2235	2267
9	16	1613	1429	1217	1167	1082	2116	2535	2529	1173	1149	1113	1098	1120	1183

Figures 12 - 13 show the corresponding intercalibration constants. The values obtained with 2011 data are compared to the existing results for year 2010.

3.5 Discussion of the results

3.5.1 Validation of selection for 2011 analysis

The event selection from 2011 analysis was checked with 2010 data to avoid conflicts in comparing the acquired intercalibration constants with previous results from 2010 data. The result of the comparison is shown in Figure 14. It is obvious, that selections of both years are the same.

3.5.2 Influence of the selection criteria

Figure 15 shows the influence of the selection *CUT* strength on the obtained mean values of the muon response. Varying the *CUT* requirement by ± 1 , the level of systematic error introduced by the selection can be estimated as:

$$\frac{Mean_{CUT+1} - Mean_{CUT-1}}{Mean_{CUT}}.$$

The obtained values of systematic errors are less than 15%.

3.5.3 Update of the selection criteria for 2011 analysis

To perform a comparison of the intercalibration constants for years 2010 and 2011, the selection criteria should be reproduced. Since some of the problematic read out channels were recovered⁸

⁸Sector 7 module 12 and sector 13 module 13 (Figures 10 - 11).

just before 2011 year data taking, *CUT* values needed to be modified with respect to the number of working channels in corresponding sector.

Table 2: *CUT* values applied for different sectors for 2010 and 2011 data.

SEC	1	2	3	4	5	6	7	8	9	10	11	12	13	14	15	16
CUT'2010	10	9	8	8	7	8	8	10	10	9	8	8	7	8	9	9
CUT'2011	10	9	8	8	7	8	9	10	10	9	8	8	8	8	9	9

3.5.4 Comparison of intercalibration constants

The behaviour of the acquired intercalibration constants in 2010 and 2011 years is the same (Figures 12 - 13). In EM modules small discrepancies are present, because of the low signals in these channels⁹ and the presence of higher signal in the reference channel in 2011 data.

4 Summary and conclusions

- Due to the location in the very forward region and nonuniform magnetic field, CASTOR calibration is challenging
- Halo muons from March-April 2011 are analyzed; the obtained statistics are comparable to 2010
- The *CUT* values are corrected according to the number of dead channels
- Intercalibration constants for 2011 spring data are calculated and they are in reasonable agreement with those from 2010
- Statistics from injection and ramp beam modes are comparable
- Systematical error introduced by selection (*CUT* value choice) is estimated to be less than 15%

To be performed:

- improvement of the selection in order to:
 - minimize *CUT* influence
 - increase the statistics
- check of new intercalibration constants with MC data

⁹The relative difference of mean values in EM modules is larger than in hadronic modules.

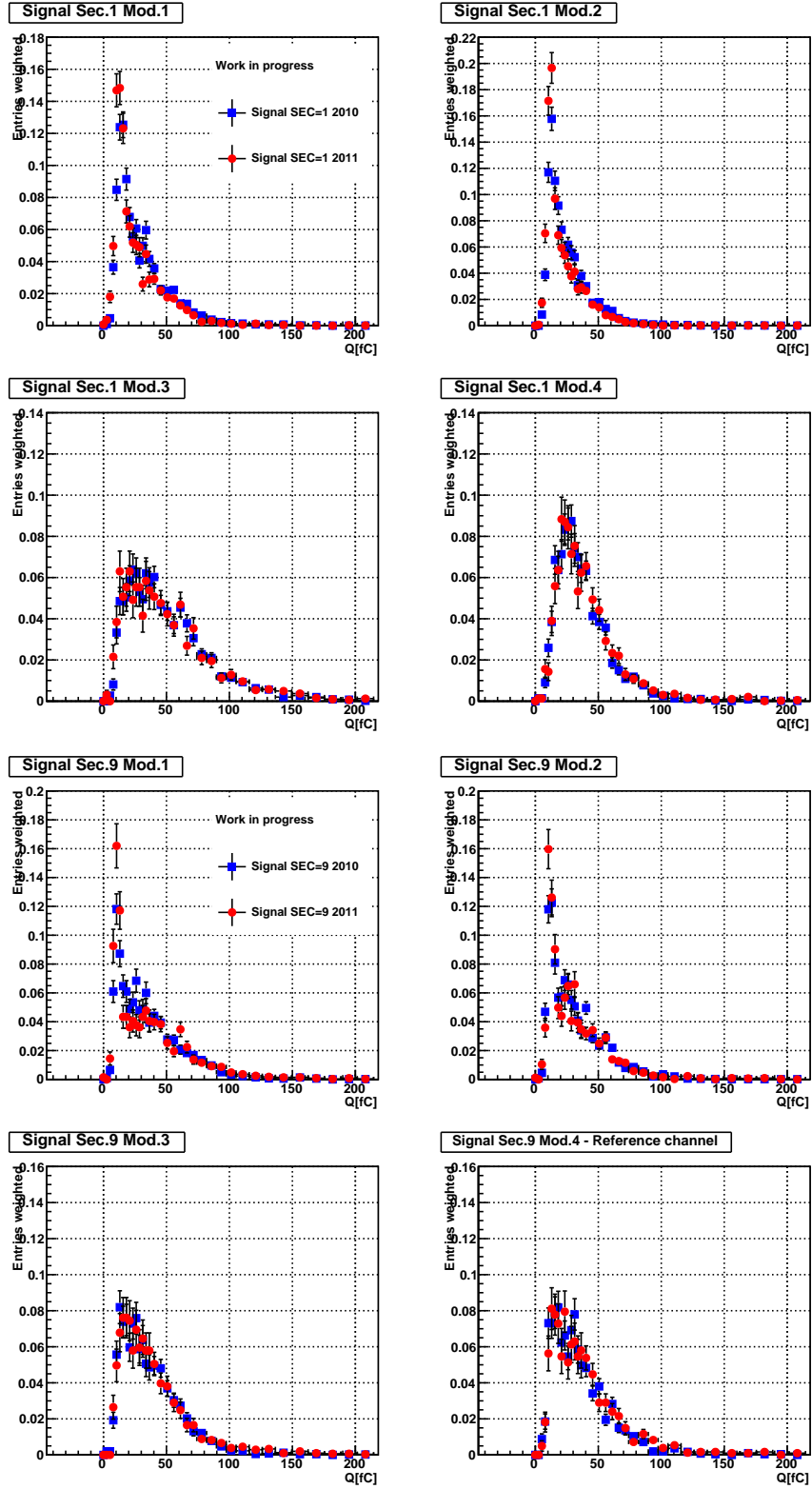


Figure 9: Example of spectra comparison for 2010 and 2011 data for the first and ninth sector. The entries are normalized to the number of events and the digitization bin width.

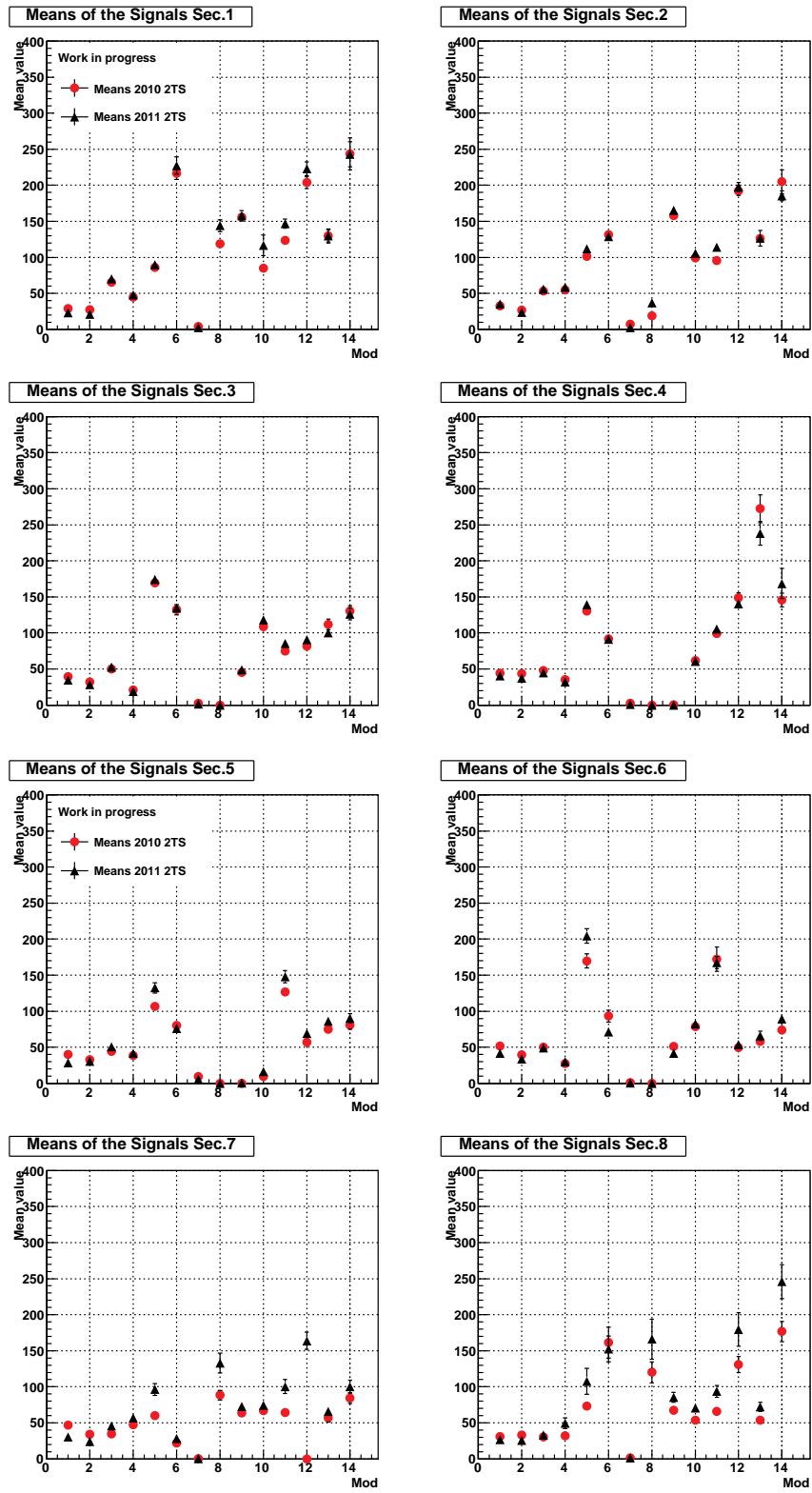


Figure 10: Mean values of a muon response obtained for 2010 and 2011 data shown for sectors 1-8.

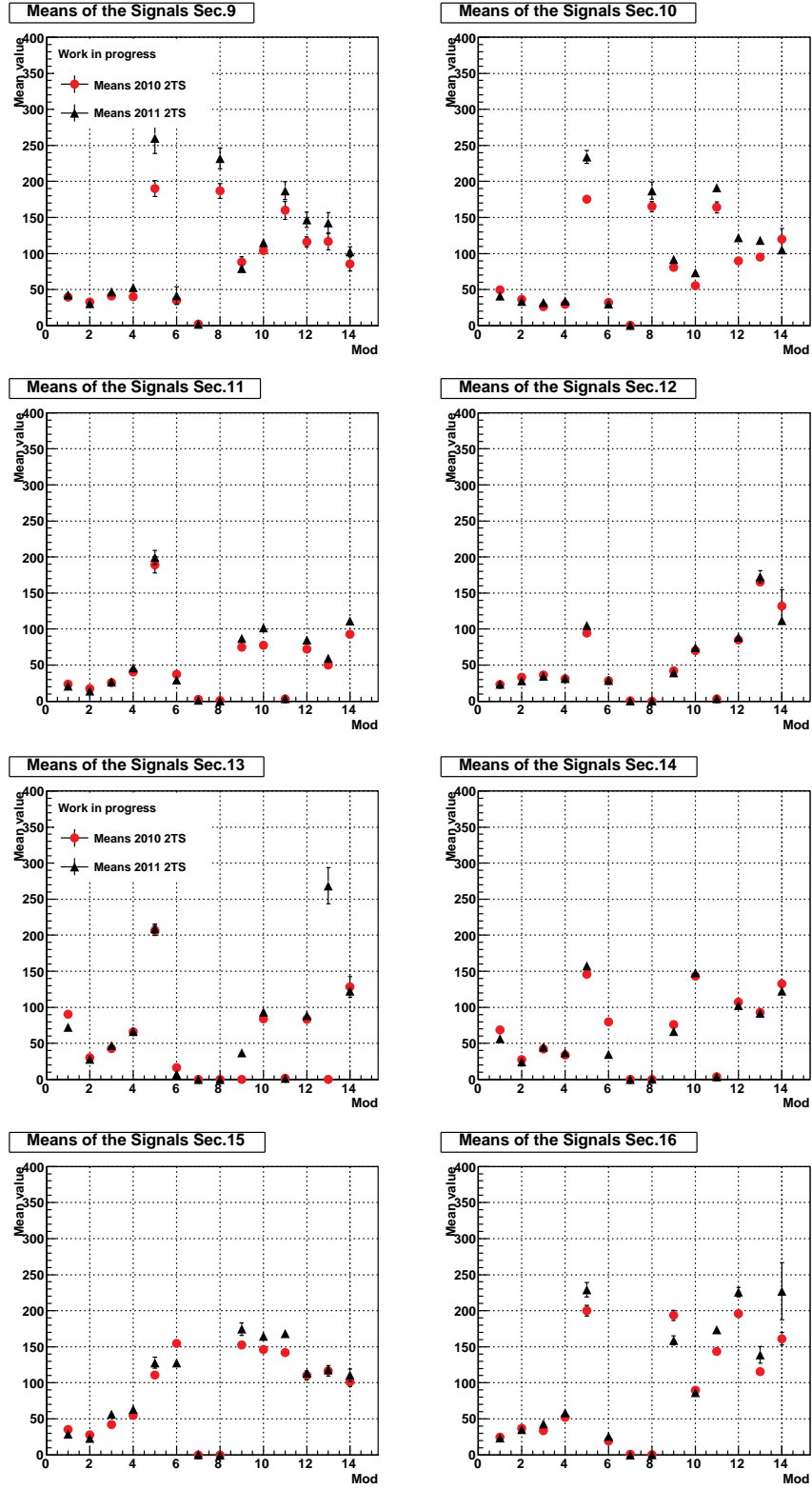


Figure 11: Mean values of a muon response obtained for 2010 and 2011 data shown for sectors 9-16.

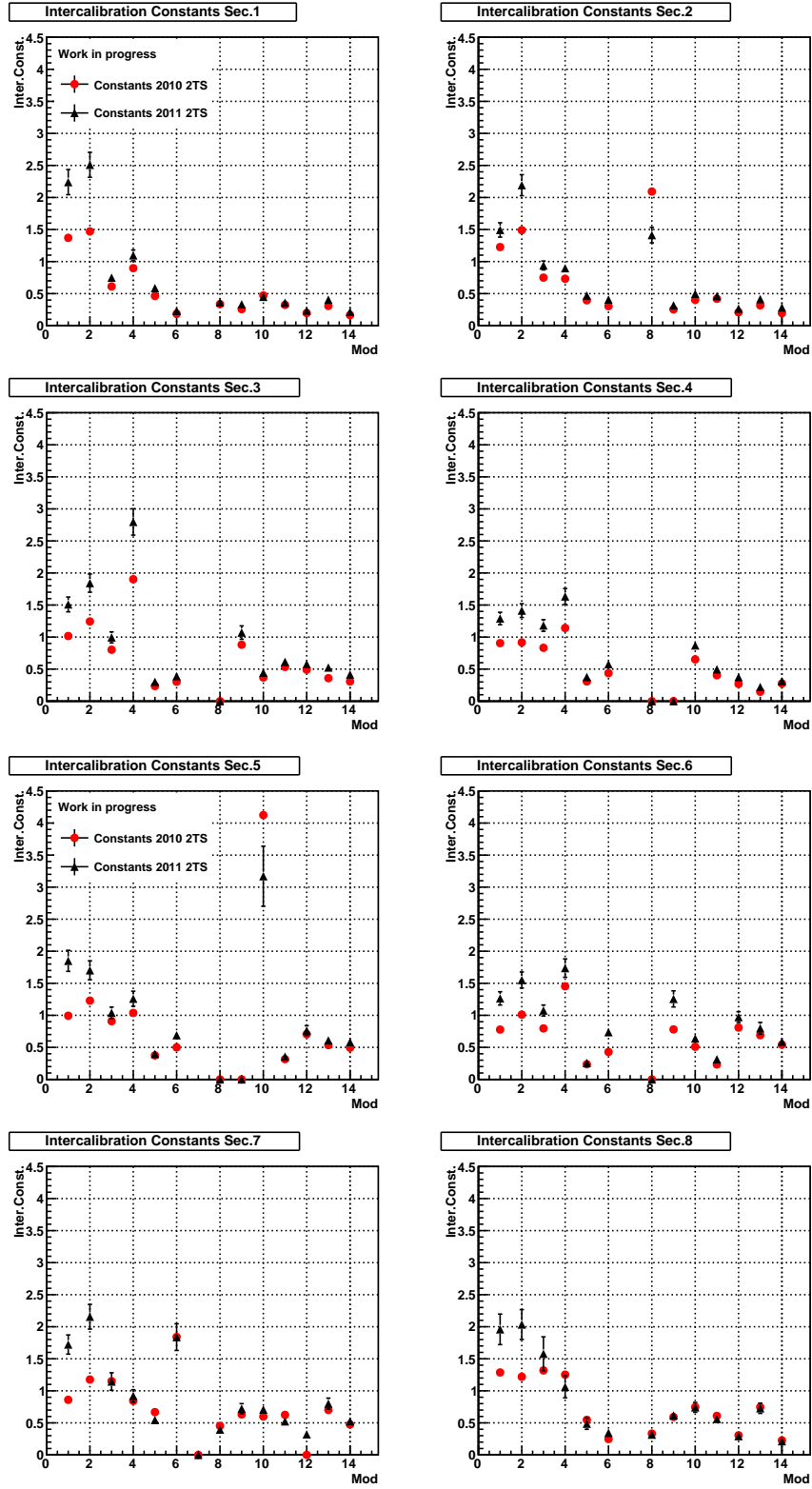


Figure 12: Intercalibration constants for sectors 1-8, obtained using 2010 and 2011 data.

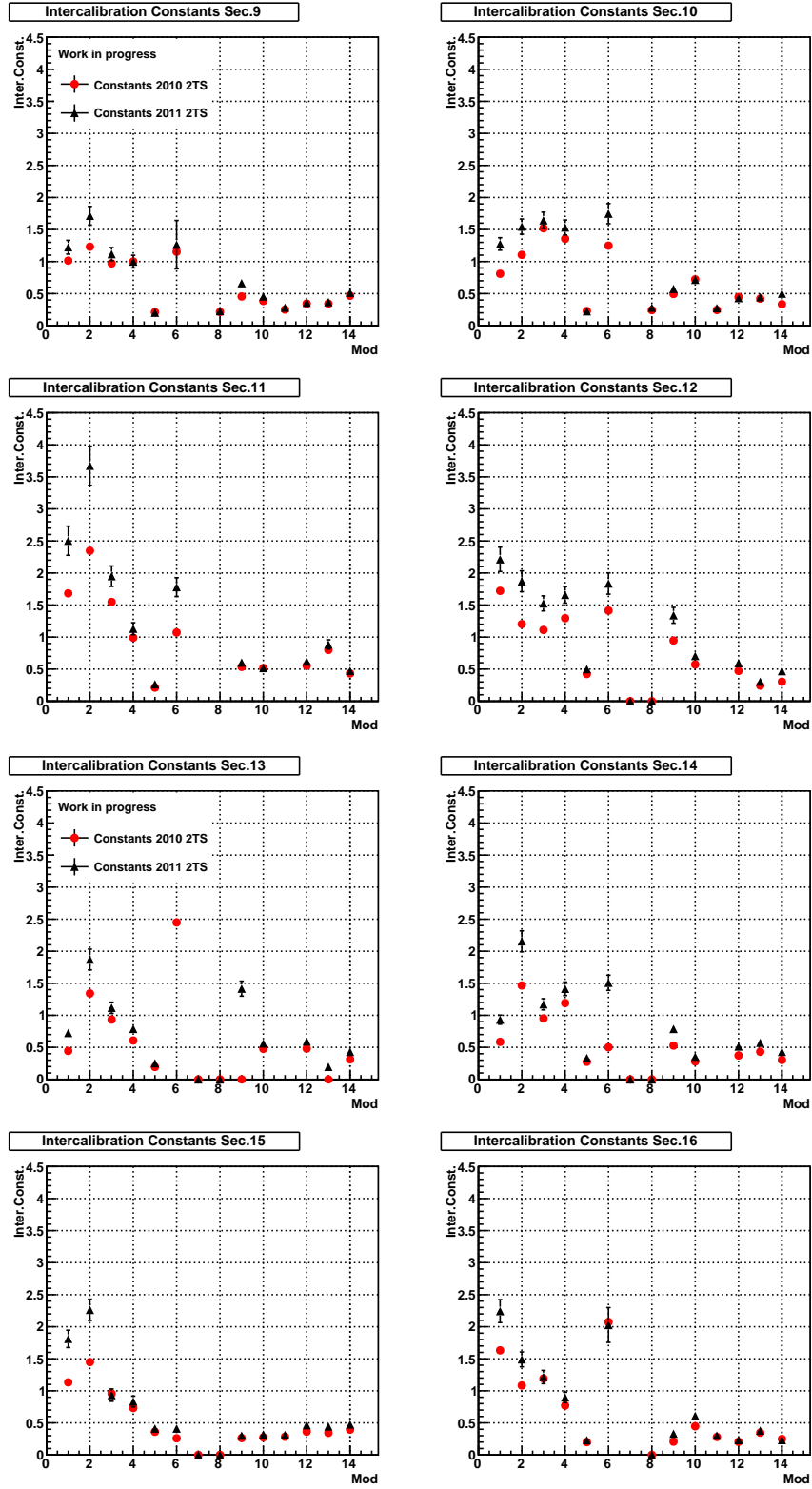


Figure 13: Intercalibration constants for sectors 9-16, obtained using 2010 and 2011 data.

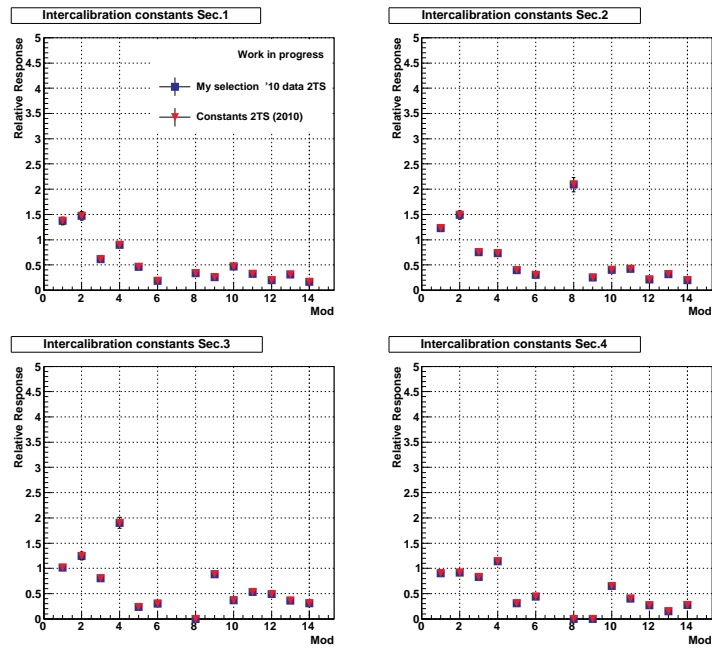


Figure 14: Comparison of 2010 intercalibration constants for sectors 1-4 with those obtained using 2011 selection with 2010 data.

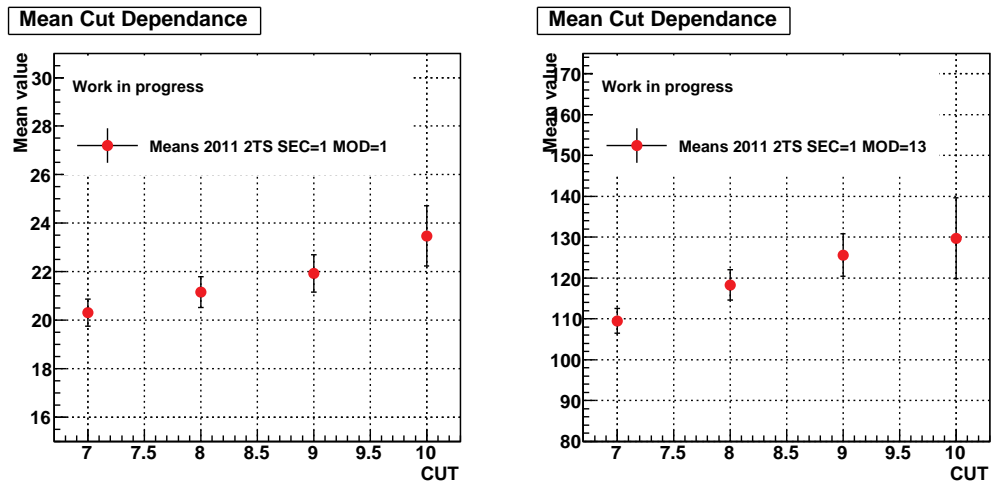


Figure 15: Dependence of mean value from *CUT*.

References

- [1] Sov. J Nucl. Phys. 15 (1972), *V.N. Gribov and L.N. Lipatov*.
- [2] Sov. Phys. JETP 45 (1977) 199, *E.A. Kuraev, L.N. Lipatov and V.S. Fadin*.
- [3] “Coherence Effects in Initial Jets at Small q^2/s ”, Nucl. Phys. B296 (1988) 49. doi:10.1016/0550-3213(88)90380-X, *M. Ciafaloni*.
- [4] “Specification for Production CMS QIE ASIC (QIE8)”, Fermilab Particle Physics/Electrical Engineering Department 2002, *Tom Zimmerman, Alan Baumbaugh, Jim Hoff, Sergey Los, Theresa Shaw*.
- [5] “Design and test beam studies for the CASTOR calorimeter of the CMS experiment”, Nuclear Instruments and Methods in Physics Research A 623 (2010) 225227, *Peter Gottlicher*.
- [6] “Machine-induced backgrounds: their origin and loads on ATLAS/CMS”, Fermilab-Conf-08-147-APC May 2008, *N.V. Mokhov, T. Weiler*.